

---

# A High Resolution Numerical Study of the Sea-Breeze Front

Steven Lambert<sup>1</sup>

*Atmospheric Environment Service, Montreal*

[Manuscript received 15 July 1974; in revised form 16 September 1974]

---

## ABSTRACT

The primitive equations are integrated numerically using a high resolution grid to investigate the sea-breeze front. Two cases of the sea-breeze front are presented; the first produced in an atmosphere with a prevailing offshore flow, and the second produced in an atmosphere initially at rest.

---

## 1 Introduction

Previous investigations of the sea-breeze circulation have been carried out using relatively coarse grids for the numerical computation and as a result, many details of the circulation remained unresolved. The feature which suffered most was the sea-breeze "front" which was completely lost by some models.

The sea-breeze front was described by Defant (1951) as developing in a synoptic regime which produces offshore surface winds which oppose the development of the sea-breeze. The zone of confluence of the synoptic wind and the onshore sea-breeze marks the sea-breeze front. Its passage at a given point is marked by an abrupt windshift and a temperature drop.

A sea-breeze front can also develop in a situation where the synoptic wind is essentially calm. In this case, the sea-breeze circulation produces its own offshore wind to form a frontal zone.

The present study is an extension of the work of Neumann and Mahrer (1971) in two respects; first an increase in the spatial and temporal resolution is used and second the sea-breeze is allowed to occur in an atmosphere *not* initially at rest.

Estoque (1961, 1962) presented similar results with a model using a coarse grid and the assumption of hydrostatic equilibrium.

## 2 The Model

Following Estoque (1961), the atmosphere is partitioned into a constant flux layer extending from the surface to a height of 50 m and a layer of transition extending from 50 m to 2075 m. This upper layer contains the rows and columns of grid points used in the numerical computation.

The governing equations for the constant flux layer are:

$$\frac{\partial}{\partial z} \left( K_z \frac{\partial U}{\partial z} \right) = 0 \quad (1)$$

$$\frac{\partial}{\partial z} \left( K_z \frac{\partial \theta}{\partial z} \right) = 0 \quad (2)$$

<sup>1</sup>Present address: McGill University, Montreal, Quebec.

where  $K_z$  = vertical eddy diffusivity  
 $U$  = total horizontal wind  
 $\theta$  = potential temperature

In order to maintain continuity in the potential temperature and horizontal wind and their vertical derivatives, it is necessary to assume that the constancy of the fluxes can be extended to the first row of grid points in the transition layer. The purpose of the constant flux layer is to provide the boundary conditions for use by the prediction equations of the transition layer. Hence, it is necessary to express the values of wind and temperature at the top of the constant flux layer in terms of the values at the surface and the values at the first row of grid points in the transition layer i.e.:

$$U_h = \beta U_{h+\Delta z} + \gamma U_0 \quad (3)$$

$$\theta_h = \beta \theta_{h+\Delta z} + \gamma \theta_0 \quad (4)$$

The subscript  $h$  refers to values at the top of the constant flux layer, the subscript  $h + \Delta z$  refers to values at the first row of grid points in the transition layer, and the subscript 0 refers to values at the surface.

Since the parameters  $\beta$  and  $\gamma$  are functions of stability, it is necessary to consider both unstable and stable regimes in the constant flux layer. The Richardson Number is used as the indicator of stability. The unstable regime occurs with:

$$Ri \leq Ri_c$$

and the stable regime with:

$$Ri > Ri_c$$

where  $Ri$  = Richardson Number  
 $Ri_c$  = a critical Richardson Number

The Richardson Number is evaluated using:

$$Ri = \frac{g(\theta_{h+\Delta z} - \theta_0)}{\bar{\theta}(U_{h+\Delta z} - U_0)^2} [h + \Delta z] \quad (5)$$

where  $g$  = acceleration due to gravity  
 $\bar{\theta}$  = average potential temperature in the constant flux layer  
 $h$  = height of the constant flux layer (50 m)  
 $\Delta z$  = vertical spacing of the grid rows in the layer of transition

The expressions for the eddy diffusivity,  $K_z$ , and the parameters  $\beta$  and  $\gamma$  were derived for the stable and unstable regimes by Estoque (1959, 1961) respectively.

For the stable regime:

$$K_z = [k_0(h + z_0)(1 + \alpha Ri)]^2 \left( \frac{U_{h+\Delta z} - U_0}{h + \Delta z} \right) \quad (6)$$

where  $k_0$  = von Karman's constant (0.4)

$z_0$  = roughness height (.02 m)

$\alpha$  = a constant (-0.03)

$$\beta = \frac{\delta_1 + \frac{\Delta z}{h + \Delta z}(\delta_1 - h\delta_2)\alpha Ri}{\delta_1 + \Delta z\delta_2} \quad (7)$$

$$\gamma = 1 - \beta \quad (8)$$

where

$$\delta_1 = \frac{1}{k_0} \log\left(\frac{h + z_0}{z_0}\right)$$

$$\delta_2 = \frac{1}{k_0(h + z_0)}$$

For the unstable regime:

$$K_z = \lambda h^2 \sqrt{\frac{g}{\theta} \left| \frac{\theta_{h+\Delta z} - \theta_0}{h + \Delta z} \right|} \quad (9)$$

where  $\lambda$  = constant (0.9)

$$\beta = 1 + 3\left(\frac{h}{h + \Delta z}\right) \left[ \left(\frac{h}{h + \Delta z}\right)^3 - 1 \right] \quad (10)$$

$$\gamma = 1 - \beta \quad (11)$$

Following McPherson (1970), the value of  $\alpha$  is taken as -0.03,  $\lambda$  as 0.9, and  $Ri_c = -0.03$ .

The equations for the transition layer are basically the two-dimensional Navier-Stokes equations for a turbulent incompressible atmosphere on the rotating earth:

$$\frac{\partial u}{\partial t} = -u \frac{\partial u}{\partial x} - w \frac{\partial u}{\partial z} - \frac{1}{\rho} \frac{\partial p}{\partial x} + fv - 2\Omega \cos\phi w + \frac{\partial}{\partial z} \left( K_z \frac{\partial u}{\partial z} \right) + K_x \frac{\partial^2 u}{\partial x^2} \quad (12)$$

$$\frac{\partial v}{\partial t} = -u \frac{\partial v}{\partial x} - w \frac{\partial v}{\partial z} - f(u - u_g) + \frac{\partial}{\partial z} \left( K_z \frac{\partial v}{\partial z} \right) + K_x \frac{\partial^2 v}{\partial x^2} \quad (13)$$

$$\frac{\partial w}{\partial t} = -u \frac{\partial w}{\partial x} - w \frac{\partial w}{\partial z} + 2\Omega \cos\phi u - \frac{1}{\rho} \frac{\partial p}{\partial z} - g + \frac{\partial}{\partial z} \left( K_z \frac{\partial w}{\partial z} \right) + K_x \frac{\partial^2 w}{\partial x^2} \quad (14)$$

$$\frac{\partial \theta}{\partial t} = -u \frac{\partial \theta}{\partial x} - w \frac{\partial \theta}{\partial z} + \frac{\partial}{\partial z} \left( K_z \frac{\partial \theta}{\partial z} \right) + K_x \frac{\partial^2 \theta}{\partial x^2} \quad (15)$$

$$0 = \frac{\partial u}{\partial x} + \frac{\partial w}{\partial z} \quad (16)$$

where  $K_x$  = horizontal eddy diffusivity  
 $f$  = Coriolis parameter  
 $\Omega$  = angular velocity of the earth  
 $u_g$  = imposed geostrophic wind  
 $\phi$  = latitude  
 $u, v, w$  = wind components.

In order to close the above system, it is necessary to include the equation of state for an ideal gas and Poisson's equation for potential temperature.

A local tangent plane co-ordinate system is used with the  $x$  axis pointing eastward, the  $y$  axis pointing northward, and the  $z$  axis pointing vertically upward. An infinitely long coastline is assumed co-incident with the  $y$  axis with the sea to the west and the land to the east.

The term  $fu_g$  in (13) allows the imposition of a large scale pressure gradient in the  $y$  direction via the steady wind  $u_g$  at the top of the transition layer.

The vertical eddy diffusivity is assumed to have an exponential decrease with height in the transition layer. McPherson's (1970) form for the height dependence is used:

$$K_z(z) = K_z(h) \exp \left\{ -m \left( \frac{z-h}{H} \right)^2 \right\} \quad (17)$$

where  $K_z(z)$  = the vertical eddy diffusivity at height  $z$

$K_z(h)$  = the vertical eddy diffusivity calculated from (6) and (9)

$m$  = constant (4.75)

$H$  = height of the top of the transition layer (2075 m.).

The value of the horizontal eddy diffusivity  $K_x$  is assumed to be constant and equal to  $500 \text{ m}^2 \text{ s}^{-1}$  in accordance with Angell, Allen and Jessup's (1971) results.

The boundary conditions at the top of the layer of transition are:

$$\frac{\partial}{\partial t}(\theta, v, u, p) = 0$$

$$w = 0$$

At the lateral boundaries the conditions are:

$$\frac{\partial}{\partial x}(\theta, u, v, p) = 0$$

$$w = 0$$

At the ground the following boundary conditions are used:

$$u = v = w = 0$$

$$T_{land} = T_0 + 16.0 \sin(15t - 110^\circ) + 4.0 \sin(30t + 75^\circ) + 0.6 \sin(45t + 66^\circ) + 0.7 \sin(60t - 115^\circ)$$

$$T_{sea} = T_0$$

$$T_{coast} = 0.5(T_{land} + T_{sea})$$

where  $t$  = time in hours measured from midnight

$T_{sea}$  = sea surface temperature

$T_{land}$  = ground temperature

$T_{coast}$  = temperature at the coastline

The form of the temperature wave used to heat the land is based on Kuo's (1968) results and gives equal land and sea temperatures at 8:00 AM.

### 3 Numerical Aspects

The equations for the layer of transition were integrated numerically on a 149 column by 29 row grid using finite differences. A forward time difference was used while the spatial terms, with the exception of the advection terms, used centered differences. The horizontal and vertical advection terms used "up-stream" differences.

Following Neumann and Mahrer (1971), the method originated by Chorin (1968) was used for solution.

A horizontal space increment of 1 km and a vertical space increment of 75 m were used. In order to maintain computational stability, a time step of 40 s was required. To control nonlinear instability, a three-point filter was applied vertically and horizontally to the potential temperature and wind fields at each time step.

### 4 Results

#### a *The sea-breeze front with an opposing offshore wind*

The initial conditions used for this integration were:

$$\begin{aligned}T_0 &= 288 \text{ K} \\u &= u_g = -3 \text{ m s}^{-1} \\v &= 0 \\ \text{surface pressure} &= 1000 \text{ mb} \\ \text{lapse rate} &= 0.0065 \text{ C m}^{-1}\end{aligned}$$

Initially, the model is integrated with equal land and sea temperatures in order to generate an Ekman Spiral in the transition layer. After this has been accomplished, the temperature wave is applied to the land. Fig. 1 shows the Ekman Spiral produced during the initialization procedure.

During the early hours of integration (time being measured from 8:00 AM), the low level offshore wind is slowly weakened. By 11:00 AM, a weak onshore flow had formed with the strongest wind occurring over the sea 4 km from the coastline. As a result, a weak sea-breeze front was present over the sea near the coast. The low level onshore flow continued to strengthen and the front began to move inland. As the front moved inland, its speed of propagation gradually diminished so that by 2:00 PM the front had become nearly stationary between six and seven kilometers inland. After 4:00 PM, the front resumed its landward motion penetrating 17 km inland by 7:00 PM. Positions of the sea-breeze front,

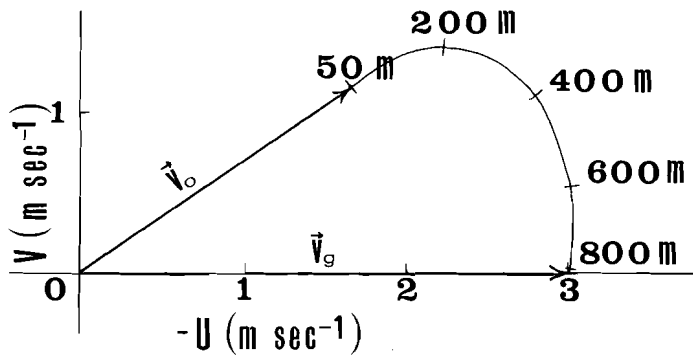


Fig. 1 Initial Ekman Spiral for the offshore wind case.  $\vec{V}_0$  is the wind at the top of the constant flux layer and  $\vec{V}_g$  is the wind at the top of the transition layer.

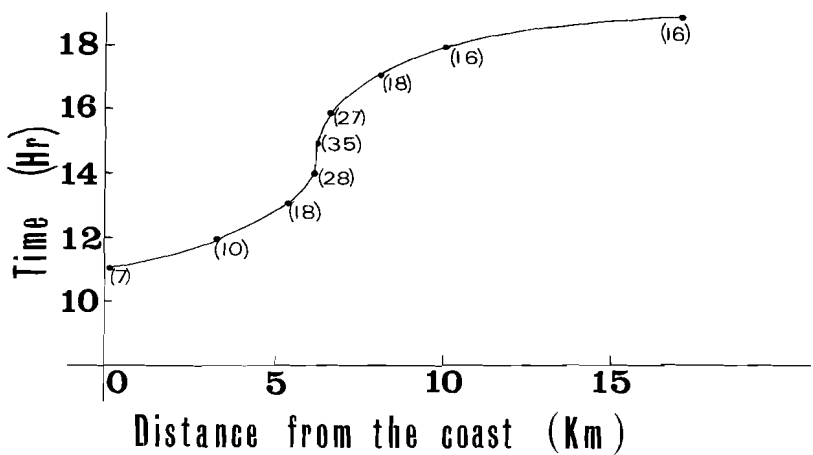


Fig. 2 Hourly positions of the sea-breeze front for the offshore wind case. Numbers in brackets are the maximum ascent in  $\text{cm s}^{-1}$  at the front.

as a function of time, are given in Fig. 2. The small figures in brackets are the strongest vertical velocities produced by the sea-breeze circulation. After 7:00 PM, rapid dissipation of the front occurred so that by 8:00 PM no onshore flow was present in the low levels.

The structure of the sea-breeze front at the time of maximum activity, 3:00 PM, is given in Fig. 3. At this time, the maximum onshore flow was  $3.0 \text{ m s}^{-1}$  with the top of the inflow layer at 450 m. An interesting feature was the strengthening of the offshore flow in the low levels just ahead of the front. As a result of the strong vertical velocity in an area which possessed a super-adiabatic lapse rate, an upward bulging of the isotherms occurred at the front producing a lowering of pressure which intensified the opposing offshore flow. Fairly strong upward vertical velocity was present above the front with the maximum of nearly  $35 \text{ cm s}^{-1}$  occurring at a height of 750 m.

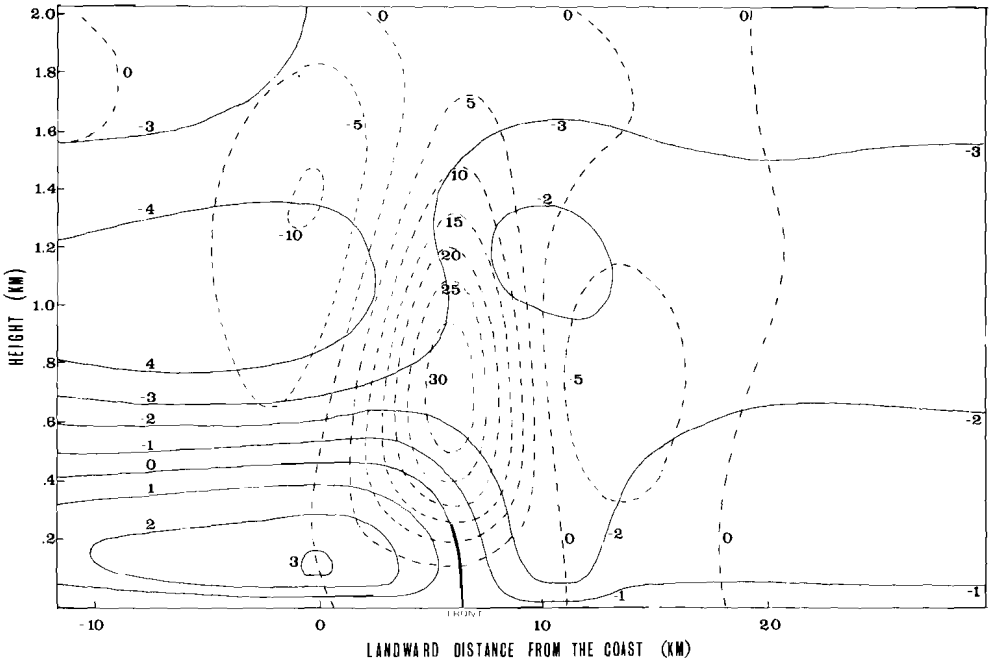


Fig. 3 The structure of the sea-breeze front at 3:00 PM for the offshore wind case. Solid lines are isopleths of the  $u$ -component in  $\text{m s}^{-1}$  and the dashed lines are isopleths of the vertical velocity in  $\text{cm s}^{-1}$ .

**b** *The sea-breeze front with a calm synoptic wind*

The initial conditions used for this solution were:

$$\begin{aligned}
 T_0 &= 288 \text{ K} \\
 u &= u_g = 0 \\
 v &= 0 \\
 \text{surface pressure} &= 1000 \text{ mb} \\
 \text{lapse rate} &= 0.0065 \text{ C m}^{-1}
 \end{aligned}$$

During the initial hours of integration, the sea-breeze developed at the coast-line and spread both landward and seaward and intensified. At 2:00 PM, an area of weak offshore winds had formed about 30 km inland producing a weak sea-breeze front 28 km from the coast. The front intensified quickly so that by 4:00 PM a well-developed front was present 30 km inland. Fig. 4 gives the structure of the front at 4:00 PM.

Fig. 5 shows a hodograph for a point on the coast and Fig. 6 shows a hodograph for a point 30 km inland. The coastal hodograph shows a continual intensification and veering of the wind while the inland hodograph shows a distinct wind shift with the passage of the front at 4:00 PM.

The front moved rapidly inland until it dissipated 60 km from the coast. Fig. 7 shows the frontal positions in time with the maximum vertical velocities.

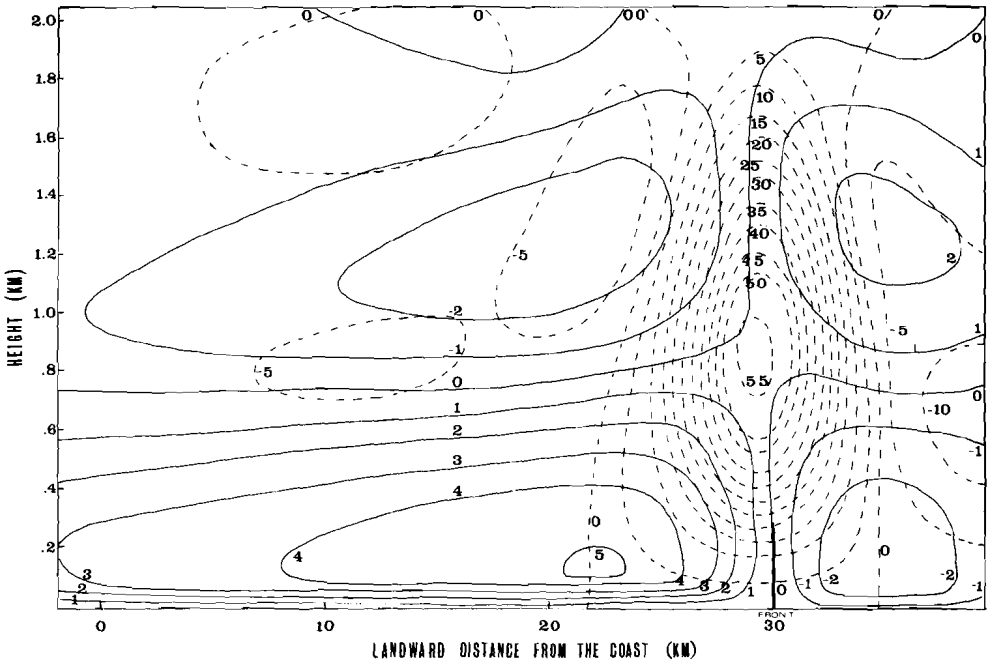


Fig. 4 The structure of the sea-breeze front at 4:00 PM for the calm synoptic wind case. Isopleths are labelled the same as in fig. 3.

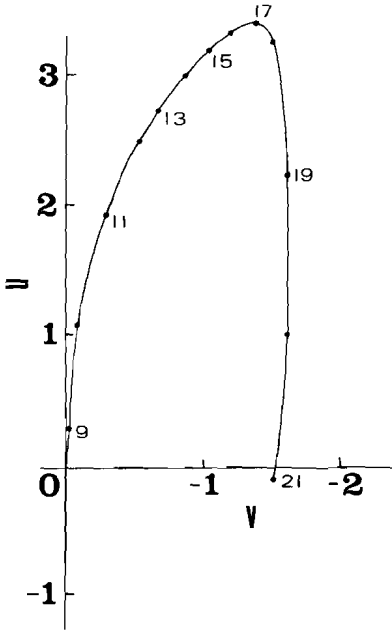


Fig. 5 Coastal hodograph for the calm synoptic wind case. The units of  $u$  and  $v$  are  $\text{m s}^{-1}$ .

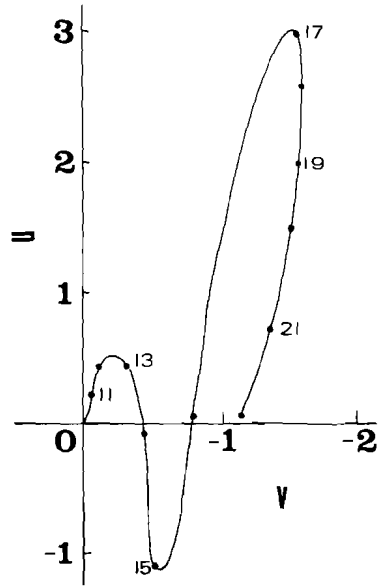


Fig. 6 Hodograph for 30 km inland for the calm synoptic wind case. The units of  $u$  and  $v$  are  $\text{m s}^{-1}$ .

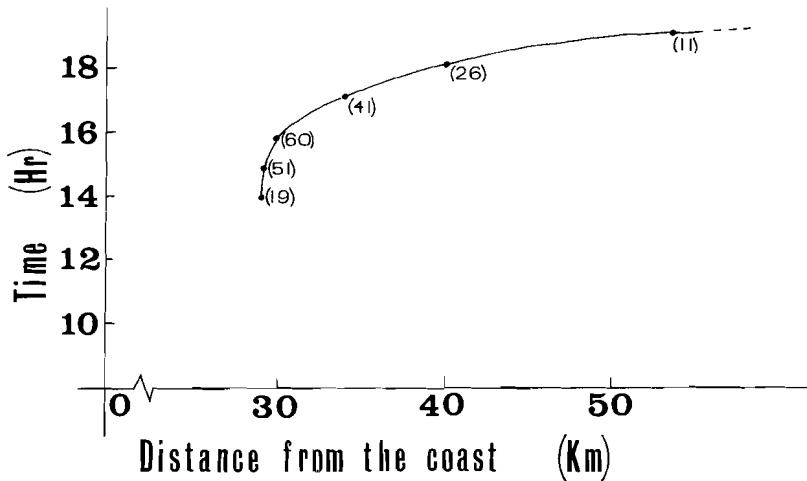


Fig. 7 Hourly positions of the sea-breeze front for the calm synoptic wind case. Numbers in brackets are the maximum ascent in  $\text{cm s}^{-1}$  at the front.

## 5 Conclusions

Observations by Lyons and Olsson (1973) of a Chicago lake breeze episode under light synoptic wind conditions show that most of the features are well-represented by the model. However, the model underforecasts the vertical velocities at the front. It was observed during numerical experimentation with the model that the vertical velocity at the front increased nearly linearly with increased horizontal resolution which indicates that a further increase in horizontal resolution would be beneficial.

## References:

- ANGELL, J. K., P. W. ALLEN, and E. A. JESSUP, 1971: Mesoscale Relative Diffusion Estimates from Tetroon Flights. *J. Appl. Met.*, **10**, 43-46.
- CHORIN, A. J., 1968: Numerical Solution of the Navier-Stokes Equations. *Math. Comput.*, **22**, 745-672.
- DEFANT, F., 1951: *Compendium of Meteorology*. Amer. Met. Soc., 658-672.
- ESTOQUE, M. A. 1959: A Preliminary Report on a Boundary-layer Experiment. *GRD Res. Notes*, **20**, AFCRC, Bedford, Mass.
- , 1961: A Theoretical Investigation of the Sea Breeze. *Quart. J. Roy. Meteor. Soc.*, **87**, 136-146.
- , 1962: The Sea Breeze as a Function of the Prevailing Synoptic Situation. *J. Atmos. Sci.*, **19**, 244-250.
- KUO, H. L., 1968: The Thermal Interaction Between the Atmosphere and the Earth and the Propagation of Diurnal Temperature Waves. *J. Atmos. Sci.*, **25**, 682-706.
- LYONS, W. A. and L. E. OLSSON, 1973: Detailed Mesometeorological Studies of Air Pollution Dispersion in the Chicago Lake Breeze. *Mon. Wea. Rev.*, **101**, 387-403.
- MCPHERSON, R. D., 1970: A Numerical Study of the Effect of a Coastal Irregularity on the Sea Breeze. *J. Appl. Met.*, **9**, 767-777.
- NEUMANN, J. and Y. MAHRER, 1971: A Theoretical Study of the Land Sea Breeze Circulation. *J. Atmos. Sci.*, **28**, 532-542.